Aeroacoustics of an Advanced Propeller Design Under Takeoff and Landing Conditions

S. Fujii,* H. Nishiwaki,† and K. Takeda†
National Aerospace Laboratory, Tokyo, Japan

Three configurations of six-bladed, 400-mm-diam, scale-model advanced propellers such as backward-, forward-, and back-forward alternately installed swept blades were tested in anechoic environments with an incoming main flow velocity up to 68 m/s. The data for the advance ratio of 0.43-1.15 were obtained in the aeroacoustic aspects. The arrangement of alternately swept blades showed the best quality among the three configurations in the spanwise circulation distribution. The forward-swept blades did not exhibit any aeroacoustic advantage. The alternately swept configuration as a tandem rotation has the potential for decreasing the sound levels at the blade passage frequencies by the dispersion of sound with neither any sacrifice of aerodynamic performance nor mechanical complexity.

Nomenclature

C = coefficient
D = propeller diameter
J = advance ratio
N = rotational speed
T = thrust
U = rotational velocity
U_0 = main flow velocity
V = flow velocity
β = pitch angle
η = efficiency
θ = ratio of ambient to standard temperature
ρ = density

Subscripts

C = correction
T = thrust
P = power
θ = tangential
0 = reference

Introduction

MANY-bladed high disk-loading propellers are being anticipated as advanced turboprops for use in the next-generation aircraft.[1,2] The aeroacoustic sector of such advanced propellers has been described freely in many publications, for example, Refs. 3-6.

The main thrust of this study was to determine experimentally the aeroacoustic aspects of an advanced propeller design under aircraft takeoff and landing conditions. Three configurations of six-bladed scale-model propellers, such as backward-, forward-, and back-forward alternately installed swept blades, were selected for a series of tests. The tests were made in anechoic environments with incoming low-speed main flow from a duct. Experimental observations of the three configurations are compared and discussed from the viewpoints of performance and noise.

Received July 2, 1985; revision received Aug. 22, 1985.

*Head, Engine Noise Group.
†Senior Researcher, Engine Noise Group.

Aerodynamic Design Methodology

The aerodynamic design was made over a scale-model propeller using the streamline curvature method,[7,8] traditionally utilized in the field of turbomachinery. In designing the compressor or turbine, the flow passage is confined and its upper wall can be considered a streamline at the boundary extremity. On the other hand, the flow around the propeller tip may be deflected inboard in passing through the rotating blades and any streamline will not be determined in advance prior to the solution of flow equations. The main feature of the streamline curvature technique is allocation of all streamlines and their renewal during iteration processes until the continuity equation has been satisfied for each streamline.

As a working equation, the radial balance of flow momentum was solved in the cylindrical coordinate system, as shown in Fig. 1. Axisymmetric flow is assumed in the whole region including intrablades, and the axial derivative term of axial velocity is neglected. The total enthalpy rise was taken into consideration during each iteration in calculating the intrablade flow, where the parabolically smooth change with the axial distance was presumed in the tangential velocity. Outside the blade region, the total enthalpy was kept constant along the streamline. The distribution of entropy rise, characteristic of flow losses, was evaluated on the basis of the front fan data.[9,10] The streamline m_0, nearest to the blade tip, was relocated until the flow solutions converged.

The aerodynamic design in this study was made to obtain the optimum performance for cruising. However, due to the capability of experimental facilities, the present tests were limited to takeoff and landing conditions.

The design point performance was evaluated at the cruising Mach number of 0.80 with a rotational speed of 250 m/s at an altitude of 10,000 m. The blade loading was selected as $shp/D^2 = 301$ kW/m^2 for cruising. The selection of blade profiles was made by use of the two-dimensional cascade data modified to include three-dimensionality, referring to the front fan and compressor test results.[3,4] The details of blades, which number eight, are shown in Table 1, where the blading at the low-solidity tip selection was determined in extrapolating the inboard profiles, since no cascade data lower than 0.40 was available in the solidity. The NACA 65-series airfoils were selected for root sections, the double circular arcs for mid-to-near tip, and NACA 16 for the tip section.

Test Facilities and Instrumentation

The 400-mm-diam scale-model propeller was placed in a $3.0 \times 5.5 \times 8.5$ m anechoic chamber with a 650-mm-diam duct

that provided a maximum flow velocity of 68 m/s at the propeller disk, see Fig. 2. A high-frequency electric motor, capable of varying the rotational speed up to 12,000 rpm at 75 kW, was used to drive the test propeller directly. To reduce the shp required for the tests under takeoff and landing conditions, the six-bladed propeller was used for the testing reported herein, although the number of blades was originally eight in the aerodynamic design.

The 27-deg aerodynamically backward-swept blades at the tip were tested first. The 27-deg forward-swept blades were manufactured next in keeping the same aerodynamic parameters as the backward blades. All blades were made of carbon-fiber-reinforced plastic. As Fig. 3 shows, a rotating cascade, composed of the backward- and forward-swept blades in sequence, was also tested under the name of cant-mixed (CM) blades. (The backward- and forward-swept blades are hereafter abbreviated as BW and FW, respectively.)

The thrust and torque were measured by strain gages fixed on a rotating shaft. To cancel side forces the strain gages were arranged to make bridge circuits. Small preamplifiers were inserted into the center of hollow drive shaft and signals were sent through a nitrogen-cooled slip ring to the outside amplifier. Prior to the tests, the static axial and twist forces were imposed on the shaft for calibration. The virtual forces when sensed at each rotational speed without blades were used to compensate the dynamic forces. A microprocessor was interfaced with the amplifier to pick up the force data and rotational speeds.

The flow data were mainly obtained from the pitot tube measurements, and partly from a 4-W argon-ion laser Doppler velocimeter (LDV) operated in a forward-scattering mode.

The acoustic measurements were made independently from the flow survey using a 12.5-mm-diam condenser microphone placed outside the jet flow 2.5 m from the center of the propeller disk, and at the same height as the shaft axis. During the measurements, most of the test rig surfaces were muffled in urethane foam to minimize the sound reflection. All data were processed making use of the on-line noise-reduction system. The runs were about 80-s long to permit satisfactory recording of the noise data, and frequency analysis was performed in the 20-Hz bandwidth. The preliminary test confirmed that the outside microphone could measure the sound emitting from a point source placed in a main-flow jet without any amplitude and ray modification due to the jet-edge shear layer up to a flow velocity of 30 m/s. The flow-on acoustic tests in the present study were therefore performed at an airspeed of 30 m/s only.

Experimental Observations and Discussion

Broadening of Sound Signature

The examples of sound spectra obtained from the BW tests at rather large pitch angles are given in Figs. 4 and 5 with and without the main flow, respectively. Figure 4 exhibits a typical signature of propeller noise consisting of the blade passage frequency (BPF) and its harmonics. Without the main flow, however, the sound pressure levels (SPL) became significantly broad and distributed around each harmonic in the spectra, as can be seen in Fig. 5. This phenomenon might be attributed to the blade flow separation because it was not observed at a small pitch angle of 30 deg. A detailed measurement of the LDV revealed that the direction of radial flow around the tip sections had opposite signs: under the static condition at such large angles, the local flow just above the propeller tip had the outboard radial mean velocity component and its maximum, 15 m/s, occurred very close to the tip leading edge, suggestive of the unstable flow recirculation from the trailing to leading edges. To make a further survey into such broadenings, the flow at the point of 20 mm outward from the midchord of tip airfoil was sensed by a miniature piezoelectric pressure transducer placed in a 5-mm-diam pitot tube. The pitot tube opening was put radially downward. A high-pass filter was used to cut off frequencies higher than the second BPF. The results of dynamic pressure spectrum analysis are

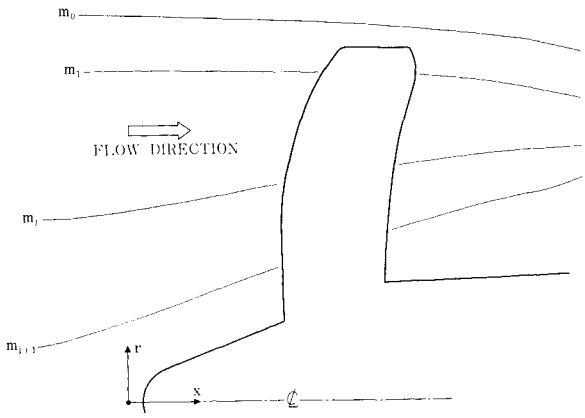

Fig. 1 Assumed streamline patterns.

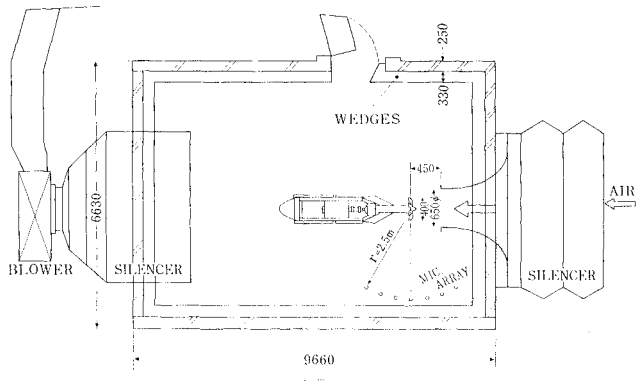

Fig. 2 Anechoic chamber, flow duct, and propeller.

Table 1. Aerodynamic and geometrical blade design parameters

	Aerodynamic			Geometrical				
Radius, mm	Helical Mach No.	Turning angle, deg	Relative flow angle, deg	Chord, mm	Camber,[a] deg	Stagger, deg	Solidity	Thickness, mm
50	0.83	4.8	14.7	77.0	2.9	10.1	1.96	15.0
116	0.94	6.1	31.2	77.0	6.9	26.1	0.85	5.0
156	1.03	6.4	39.2	74.0	8.3	33.6	0.60	4.0
192	1.12	4.9	45.2	60.0	5.3	39.7	0.40	3.0
200	1.16	2.3	46.7	58.0	—[b]	—[b]	0.37	2.9

[a]The camber angle of 25 deg is equivalent to the lift coefficient of 1.0. [b]The values at two radii of 187 and 192 mm were linearly extrapolated to determine the camber and stagger angles at the tip section since no cascade data were available in the solidity lower than 0.40.

demonstrated in Figs. 6 and 7. When the propeller was operated with the main flow on, the dynamic pressure changed very regularly as each blade passed, see Fig. 6. However, without the main flow at the large pitch angle, each blade produced the unstable and unreproducible waves per one revolution due to the blade flow separation, Fig. 7. Such irregularities might generate a sound signature unrelated with the rotational speed as a result of flow/acoustics coupling, which, in turn, yielded the broadening of the sound pressure spectra extended around the BPFs.

Comparison of Three Configurations

Aerodynamic Aspects

The blade rotational Mach number plays an important role in the noise emission, whereas the helical Mach number relative to the blade surface becomes a major parameter in considering the aerodynamic performance. Therefore, to evaluate both aspects of noise and performance rigorously, the corrective rotational speeds N_C may be taken as a common criterion for the aeroacoustic comparison, that is, on the N_C constant basis. As is well known, N_C is defined as the mechanical rpm N divided by $\sqrt{\theta}$, where θ is the ambient/standard temperature. With this rotation, for example, the thrust coefficient can be expressed as $C_T = T/\rho_0 N_C{}^2 D^4$ in terms of a reference density ρ_0, and N_C instead of $T/\rho N^2 D^4$.

Figures 8 and 9 show the variations of C_T, C_P, and η with reference pitch angles at constant $N_C = 8000$ and 10,000 rpm, respectively. The most pronounced superiority of the CM over the BW and FW was marked at $\beta_{0.75} = 36$ deg and $N_C = 8000$ rpm. The corresponding tangential velocity distributions along the radius are drawn in Fig. 10. The data set was obtained from the pitot tube traverses at the downstream sections of 15 mm from the BW and CM blade trailing edges, and 25 mm from the FW. The velocity imparted in the tangential direction is considered proportional to the flow circulation at each blade element. It is shown that the CM gave rise to a much more moderate distribution of circulation along the blade span than the BW and FW. In the configuration of the BW, most circulation was concentrated toward the tip section, which might be unfavorable in viewing the flow separation. It was unexpected that the FW had the inferior characteristics in the tangential velocity distribution, particularly with little circulation obtained near the propeller tip.

The outlet flow angle relative to the rotating blade as well as the turning angle as a result of passing through the blade row are plotted for the BW and FW in Fig. 11. The zero-turning zone, which usually extended inboard from the tip, was much larger in the FW than the BW.

The insufficient quality of the FW in the total pressure ratio was again observed at an advance ratio of 1.15, which was

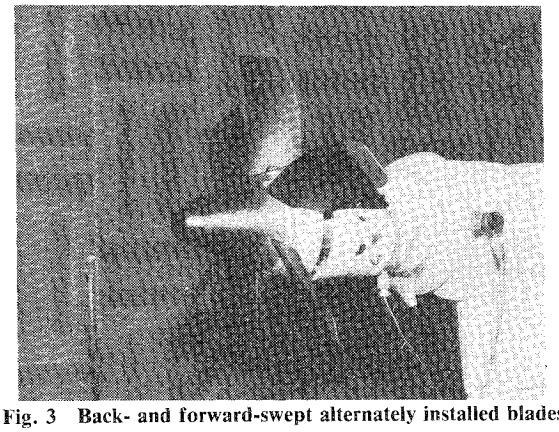

Fig. 3 Back- and forward-swept alternately installed blades.

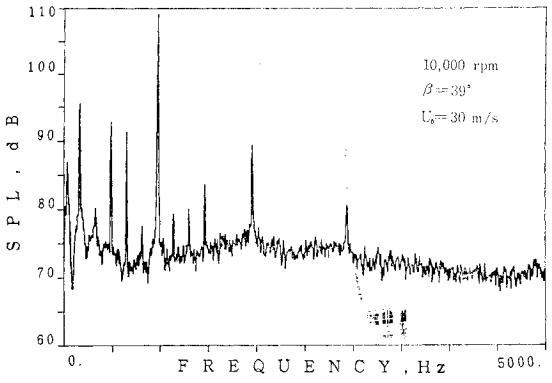

Fig. 4 Sound pressure spectrum with main flow on.

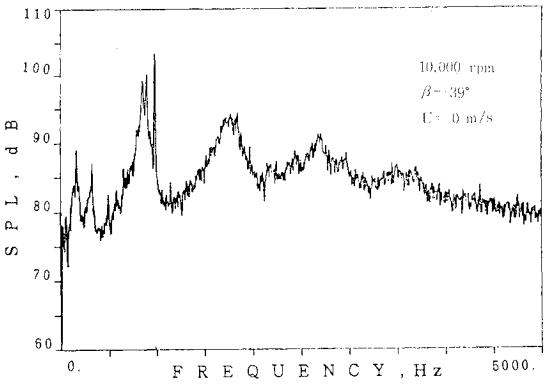

Fig. 5 Sound pressure spectrum under static conditions.

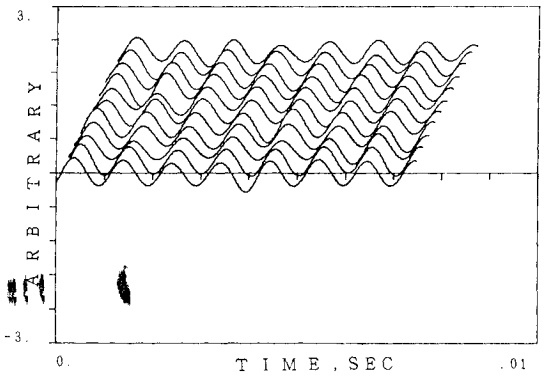

Fig. 6 Flow pressure waves from each blade with main flow on.

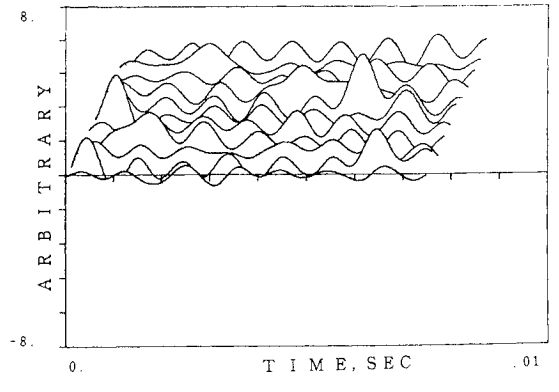

Fig. 7 Flow pressure waves under static conditions.

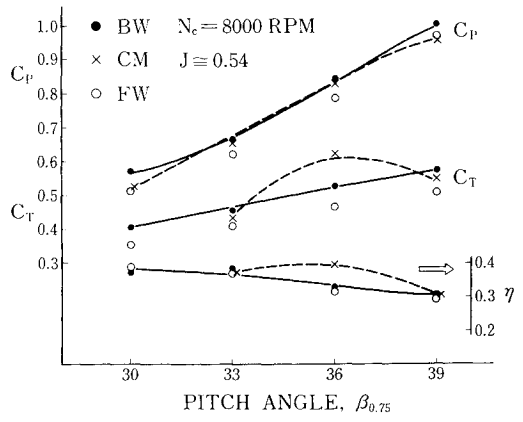

Fig. 8 Power, thrust, and efficiency variations with pitch angles for $J = 0.54$.

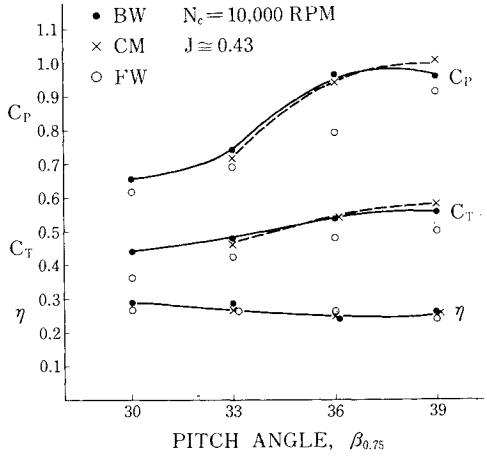

Fig. 9 Power, thrust, and efficiency variations with pitch angles for $J = 0.43$.

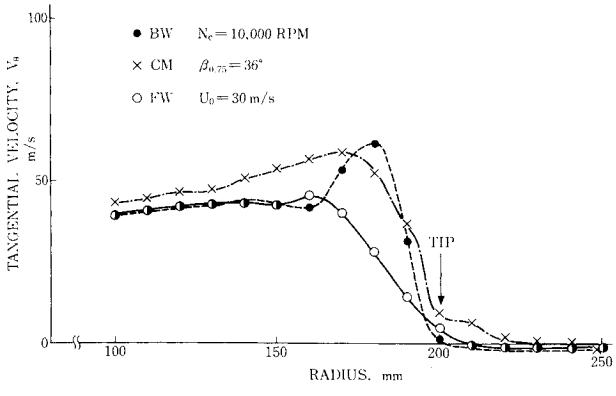

Fig. 10 Comparison of tangential velocity spanwise distributions.

realized by an increase of duct flow velocity up to 68 m/s, see Fig. 12. It is noted that the total pressure rise can be given by the enthalpy change UV_θ accounting for flow losses across the blade row. It was found that the difference in the spanwise distribution became minimal between the CM and BW, as the advance ratio increased from 0.43 to 1.15 but with still poor performance toward the tip sections in the FW.

In summarizing the aerodynamic characteristics, the CM showed the best results among the three configurations tested at the small advance ratios (0.4-0.5) with rather large angles of attack (20-30 deg), while at the moderate advance ratio (1.15) with the angle of attack less than 15 deg, there did not exist any remarkable difference between the CM and BW

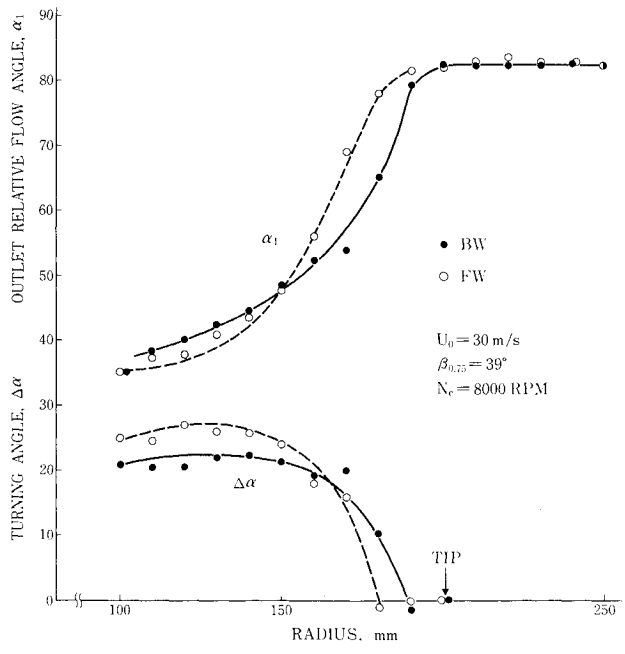

Fig. 11 Flow angle comparisons for back- and forward-swept blades.

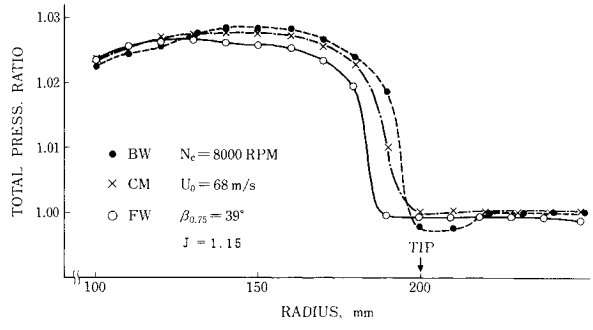

Fig. 12 Comparison of total pressure spanwise distributions.

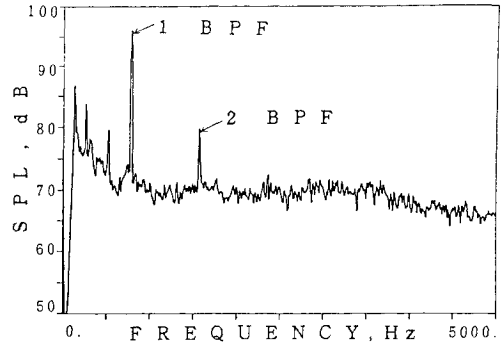

Fig. 13 Noise spectrum of backward-swept blade at $N_C = 8000$ rpm, $U_0 = 30$ m/s, and $\beta_{0.75} = 36$ deg on the sideline.

aerodynamic performance. It can be mentioned that the CM worked as though the two rows of blades were rotating in tandem from the midsection to the tip section. Such an arrangement may have the advantage of substantial resistance to flow separation at high angles of attack. Further research is needed to clarify the flow mechanism inherent in the CM configuration, since the blending of back- and forward-swept blades produced mild and favorable spanwise circulation in contrast with the FW inferiority.

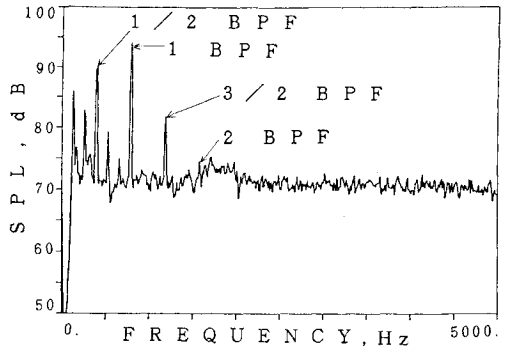

Fig. 14 Noise spectrum of alternately swept blades under the same conditions as Fig. 13.

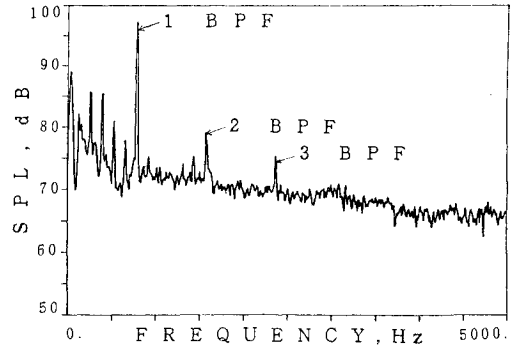

Fig. 15 Noise spectrum of forward-swept blades under the same conditions as Fig. 13.

Acoustic Aspects

The noise facets of three configurations are exhibited in Figs. 13-15. It is of interest to note the sound characteristics of the CM. The peak levels were newly detected at 1/2 and 3/2 BPF, besides the first BPF, and instead the 2 and 3 BPF levels became obscure, see Fig. 14. The decrease of about 2 dB in the first BPF sound level was discerned in comparison with the BW and FW. It can be said that the sound pressure levels were dispersed due to the blend of opposite swept blades. The corresponding radiation patterns of the first BPF sound pressure are shown in Fig. 16. The substantial decrease of 10 dB was measured upstream 30 deg for the CM relative to the BW.

The pressure waves during the successive blade passes are indicated in Figs. 17 and 18 for the sideline measurement. The specific character of the CM was again noted. It can be explained that the noise emission from the axially different source positions in the mixed swept blade arrangement might cause the phase cancellation and amplification of the sound pressure waves. It also may be understood that the noise emission from a set of three forward-facing blades and three aft-facing blades produced the new peak levels at 1/2 and 3/2 BPF. Mechanisms common to all six blades generated the first BPF, at which we might also have the second harmonics of three-bladed phenomenon.

The evaluation and comparison of noise aspects should be made by taking into account the levels of thrust or power coefficients because each harmonic sound level is roughly proportional to the thrust and drag magnitude. With this kept in mind, a thorough check of all acoustic data taken during the testing indicates neither advantage nor disadvantage of the FW over the others. At high angles of attack, the CM has a considerable advantage in both aerodynamic and acoustic aspects: moderate spanwise circulation and sound intensity dispersion. It is tentatively concluded that the CM has the

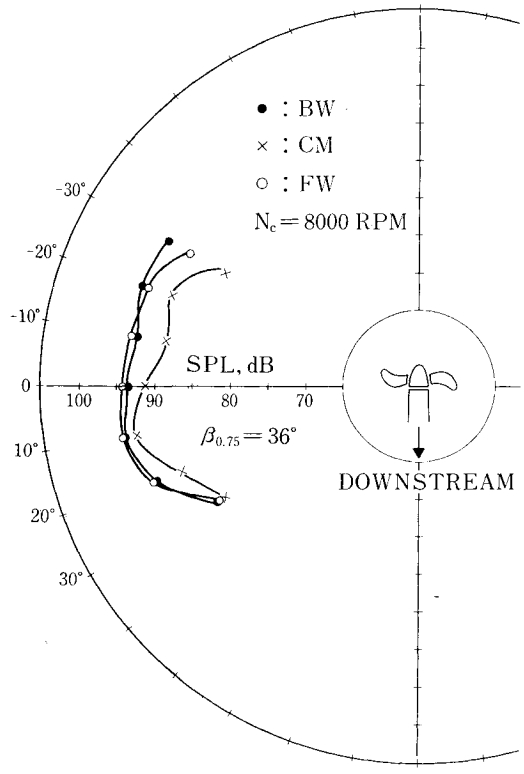

Fig. 16 Comparison of radiation directivities for the first BPF.

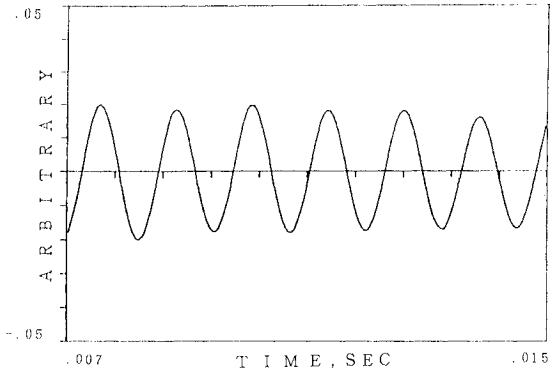

Fig. 17 Sound waves with time for backward-swept blades on the sideline.

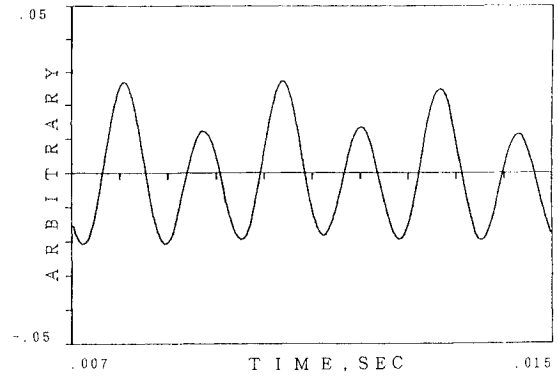

Fig. 18 Sound waves with time for alternately swept blades on the sideline.

potential for decreasing the sound levels in dispersing the sound intensity at each BPF without suffering any aerodynamic performance deterioration. Any additional mechanical weight and complexities are not required in the CM tandem rotation. However, from an engineering standpoint, it is important for the CM tandem rotation to trade off the sound dispersion at the defined frequencies for the noise at new frequencies in the practical application.

It is speculated that the characteristics of softening the BPF's peak sound by the CM may continue in the transonic regime, although the aerodynamic advantage of the CM over the BW no longer will be enjoyed at the design angle of attack.

Conclusions

1) The three configurations of the swept angles of six-bladed, carbon-fiber advanced propellers were tested in the anechoic environments with the main flow imposed up to 68 m/s.

2) Under the static condition at the large angle of attack, the propeller tip flow separated with the outboard velocity component attendant, which yielded the broad sound spectra distributed around the BPFs.

3) At an advance ratio of 0.4-0.5 the CM showed the best quality among the three configurations in the spanwise circulation.

4) As the advance ratio increased up to 1.15, the aerodynamic advantage of the CM over the BW was no longer obtained, while the FW still had insufficient performance near the tip.

5) It is tentatively concluded that the CM arrangement as the tandem rotation has potential for abating the sound intensity at the BPFs with neither any sacrifice of performance deterioration nor mechanical complexities attendant. However, the sound dispersion should be traded off for the new peak levels from a practical point of view.

6) Further study is strongly recommended to perform the same tests as those reported herein in the transonic regime, where the extended use of the streamline curvature technique and cascade data made in the present design also will be evaluated.

Acknowledgments

The authors would like to acknowledge the Environment Protection Agency of Japan for the financial support of the present study. The authors are also grateful to Messrs. A. Ohara and Y. Kawakami, Sumitomo Precision Products, for helpful discussion. Ms. Y. Sasaki contributed considerable assistance in typing the manuscript.

References

[1]Gatzen, B.S., "Turboprop Design Now and the Future," AIAA Paper 82-452, Aug. 1982.

[2]Ludemann, S.G., "Prop-Fan Powered Aircraft—An Overview," SAE Tech. Paper 820957, Aug. 1982.

[3]Black, D.M., Menthe, R.W., and Wainanski, H.S., "Aerodynamic Design and Performance Testing of an Advanced 30 deg Swept, Eight Bladed Propeller at Mach Numbers from 0.2 to 0.85," NASA CR-3047, Sept. 1978.

[4]Metzger, F.B. and Rohrbach, C., "Aeroacoustic Design of the Prop-Fan," AIAA Paper 79-610, March 1979.

[5]Block, P.J.W. and Martin, R.M., "Results from Performance and Noise Tests of Model Scale Propellers," SAE Tech. Paper 830730, April 1983.

[6]Dittmar, J.H., Jeracki, R.J., and Blaha, B.J., "Tone Noise of Three Supersonic Helical Tip Speed Propellers in a Wind Tunnel," NASA TM-79167, June 1979.

[7]Novak, R.A., "Streamline Curvature Computing Procedures for Fluid-Flow Problems," *Transactions of ASME, Journal of Engineering for Power*, Vo. 89, Oct. 1967, pp. 478-490.

[8]Fujii, S. and Uno, T., "Streamline-Curvature Approach to Duct-Flow Problems," National Aerospace Lab., Tech. Rept. TR-140, Sept. 1967.

[9]Fujii, S., Nishiwaki, H., and Gomi, M., "Design and Performance Comparison of Three High-Speed Fans," *Proceedings of the 1983 Tokyo International Gas Turbine Congress*, Vol. 2, Oct. 1983, pp. 369-376.

[10]Fujii, S., "Acoustics and Performance of High-Speed, Unequally Spaced Fan Rotors," *Transactions of ASME, Journal of Engineering for Power*, Vol. 102, Jan. 1980, pp. 19-27.